Temporal imaging of mine-induced stress change using seismic tomography

M.J. Friedel[a,*], D.F. Scott[b], T.J. Williams[b]

[a] *University of Minnesota, Department of Geological Engineering, Minneapolis, MN, USA*
[b] *US Department of the Interior, Bureau of Mines, Spokane Research Center, Spokane, WA, USA*

Received 9 April 1996; accepted 9 September 1996

Abstract

In an effort aimed at monitoring mining-induced stress changes that may influence ground failure, the US Bureau of Mines conducted a series of active 3-D seismic tomographic surveys at the Homestake (Lead, South Dakota) and Lucky Friday (Mullan, Idaho) mines. Existing rock bolts were used to mount geophones and as strike points for introducing seismic energy using a 3.6 kg sledge hammer. Travel time measurements were recorded spanning up to 160 m between drifts at several levels. The tomographic uncertainty was minimized by computing iso-velocity surfaces of constant probability based on statistics from multiple reconstructions and a threshold criteria. Periodic imaging using tomographic velocity surfaces demonstrated that temporal and spatial changes in the local stress field occurred in response to ground failure and stope advancement at a gold and silver mine, respectively.

Keywords: Temporal imaging; Mine-induced stress; Seismic tomography; Geophysics

1. Introduction

1.1. Problem

Mining activity in the western US and elsewhere reaches depths of more than 2 km. The lithostatic stress at this depth is significant, on the order of 50 MPa, and mining activity causes substantial perturbation of the ambient stress field. Removal of ore and fracturing of adjacent material by blasting results in the transfer of stress to mine pillars and other intact rock volumes. Concentration of stress to levels exceeding the strength of rock and/or geological discontinuities often results in a catastrophic and generally unpredictable release of strain energy, e.g., Richter magnitudes of 2.2 and 3.5 in the Homestake and Coeur d'Alene mining districts, posing grave danger to miners and increasing production costs due to clean up, lost time and the need for additional rock support.

Although a variety of countermeasures are in use in these rupture-prone mines, no method has proven entirely reliable. Conventional countermeasures can be passive, e.g., observation of temporal/spatial sequences of rock mass failure using microseismic monitoring, or active, e.g., excavation sequencing, application of counter stresses through bolt installation, and/or destressing through a drill and blast sequence. Despite the

* Corresponding author.

use of these countermeasures, catastrophic ground failure continues, often with no microseismic precursors (Blake and Cuvelier, 1990). As mining proceeds to greater depths, the unabated failure of ground into underground mine openings will remain a persistent safety hazard and an impediment to production. Presently, there remains the need to develop a simple, rapid, and cost-effective tool for periodic imaging of mine structures under the full range of stress conditions. One such promising "high resolution" geophysical technology is active 3-dimensional seismic tomography.

1.2. Approach

The rationale for using seismic tomography to aid in mapping mine-induced, stress-related phenomena was based initially on laboratory observations of the interrelationship between velocity and stress (e.g., Thill, 1982; Radcliffe et al., 1986). Recently, Friedel et al. (1995b) demonstrated that a good visual correlation existed between a simple mechanical model and velocity distribution derived from a 3-D underground tomographic survey. In general, both laboratory and field observations suggest that high- and low-velocity regions in a homogeneous rock mass may be indicative of elevated and diminished stress, respectively. These findings are further supported by a numerical study in which structural heterogeneities, e.g., fractures were found to enhance the sensitivity of velocity to relative changes in magnitude of in situ stresses. In the event that normal stress across a geological discontinuity is high, the in situ velocity may approach that for intact rock.

To date, a number of researchers have applied seismic tomography to investigate mine-induced stress. Early studies focused on coal measure rocks; a comprehensive review is provided by Gibowicz and Kijko (1994). While encouraging, these studies were limited by the application of 2-D linearized solutions, insufficient raypath coverage (sampling and viewing angles) and inability to impose explicit constraints. Recent studies have improved on these early efforts by incorporating curved ray tracing, various constraints, and extension to 3-D (Young and Hill, 1985; Young, 1993; Friedel et al., 1992, 1993, 1995a,b, 1996; McCreary et al., 1992; Maxwell and Young, 1992; Young and Maxwell, 1992; Westmann et al., 1994; Jackson and Tweeton, 1996). This paper describes the use of 3-D seismic tomography for monitoring mining-induced stress changes at the Homestake gold mine and Lucky Friday silver mine.

2. Homestake mine

2.1. Geology

The Homestake gold mine, owned and operated by Homestake Mining Company, is located in Lead, South Dakota. The geology is typified by altered Precambrian metamorphic rock occurring within a Tertiary east–west trending arch. The host rock is the Homestake formation, a green-gray chlorite schist. Accessory rock types include quartzites and phyllites of the Ellison and Poorman formations, respectively. All three formations contain about 15% disseminated sulfides, such as pyrrhotite and arsenopyrite.

Unconfined mechanical and sonic measurements conducted on samples of these rock types in the laboratory indicate a weak lithological variation in elastic properties (Johnson et al., 1993). In particular, the compressional wave velocity varied less than 10% between rock types. In this case, those tomographically-reconstructed velocities that deviate by $1\ \mathrm{km\,s^{-1}}$ (± 2 S.D.) from the average $4.34\ \mathrm{km\,s^{-1}}$ laboratory p-wave velocity may be attributed to mining-induced, stress-related phenomena.

2.2. Mining activity

Currently, mining activity at the Homestake occurs to a depth of 2438 m (8000 level). The tomographic study site occupies a block of ground between 2164 (7100 level) and 2210 m (7250 level) depths (the level designation is equivalent to depth in feet from the surface). Mining of the Homestake formation occurs within the study region in the form of mechanized cut-and-fill and vertical crater retreat. Ramps provide access to the stopes which

vary in size depending on the ore body size. Ore extraction generally proceeds in an upward direction in lifts that are about 3 m thick. Following extraction, the stopes are backfilled with a low-modulus mix of sand and waste rock in an attempt to mitigate ground stability problems. Fig. 1 provides a 3-dimensional southeasterly view of various mine features including the 7100 and 7250 level drifts, backfilled stopes, and approximate extent of ore reserves.

3. Lucky Friday mine

3.1. Geology

The Lucky Friday mine, owned and operated by Hecla Mining Company, is located in the Coeur d'Alene Mining District near Mullan, Idaho. The two primary rock formations at the mine are the argillitic St. Regis, and the Revette, composed primarily of vitreous quartzite with thinly (1 cm to tens of cm) interbedded sericitic quartzite and argillite (Scott, 1993). The steeply southward-dipping (about 80°) east–west trending, Lucky Friday vein is composed of silver–lead–zinc that continues to depths of more than 1.62 km. In the region of study, the Lucky Friday vein bifurcates into what are known locally as the hanging and footwall veins. Unconfined laboratory sonic measurements conducted on intact samples of vitreous quartzite revealed that p-wave velocities average about 4.45 km s^{-1}.

3.2. Mining activity

The study region, known as the "remnant ore pillar," represents a block of ground that is vertically defined by previous mining activity delimited by the 1493 (4900 level) and 1555 m (5100 level) depths. The width of this remnant structure is defined by the lateral extent of crosscuts on the two levels (e.g., 4900, 87, 93 and 95; and 5100: haulage, 88, 92), while its length is defined by the distance spanning the outer most crosscuts (Fig. 2). In this region, bedding strikes east–west, essentially parallel to the vein, and dips south–southwest at approximately 60°. The N40°W trending South Control fault terminates the western edge of the Lucky Friday vein. At the time of the first tomographic survey, mining activity using

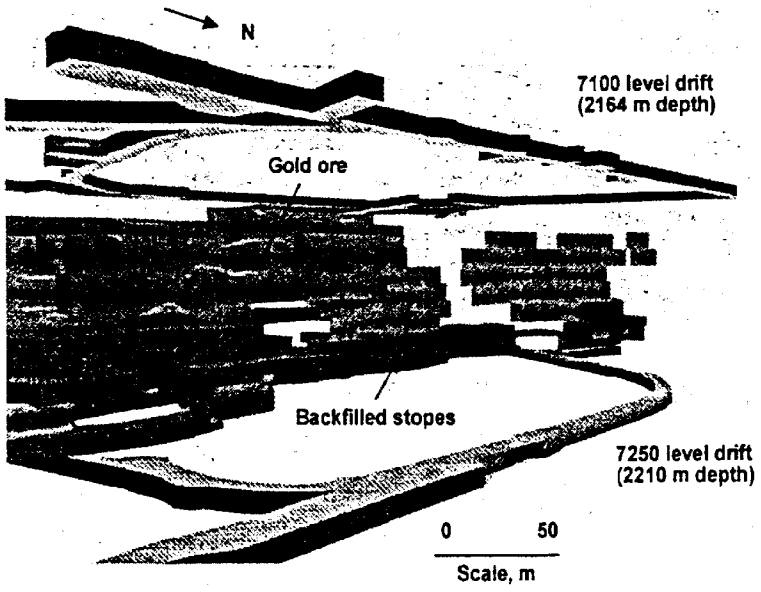

Fig. 1. Three-dimensional southeasterly view of Homestake mine study site.

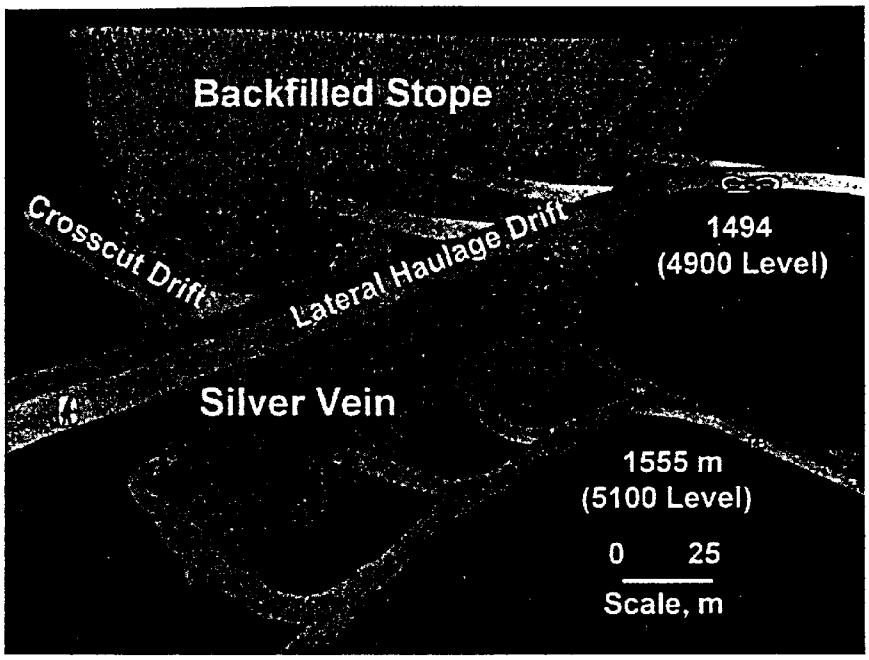

Fig. 2. Three-dimensional northeasterly view of Homestake mine study site.

underhand cut and fill was engaged at a depth of 1540 m (5150 level). By the second survey, mining had advanced downward by about 10 m to a depth of 1540 m. These stopes are also backfilled with a low modulus cement-sand. Fig. 2 provides a 3-dimensional northeasterly view of the 4900 and 5100 level drifts and crosscuts, backfilled stopes and approximate extent of remaining silver ore.

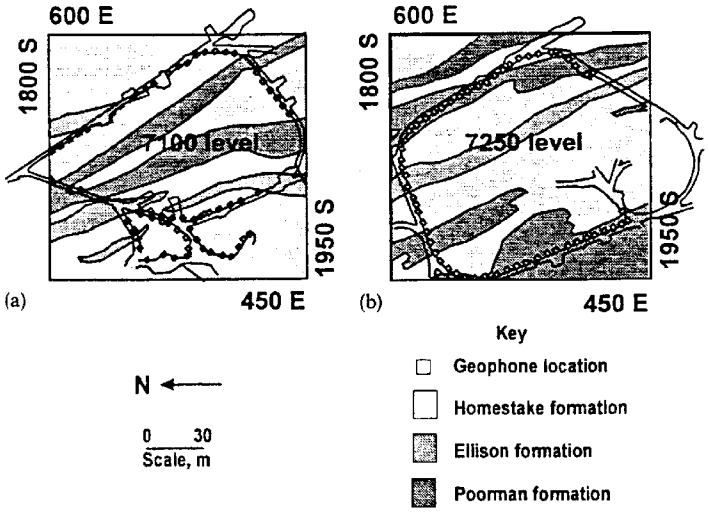

Fig. 3. Plan view of geophone stations and mine drifts: (a) 7100 level (2164 m) Homestake mine; (b) 7250 level (2210 m) Homestake mine; (c) 4900 level (1494 m) Lucky Friday mine; (d) 5100 level (1555 m) Lucky Friday mine.

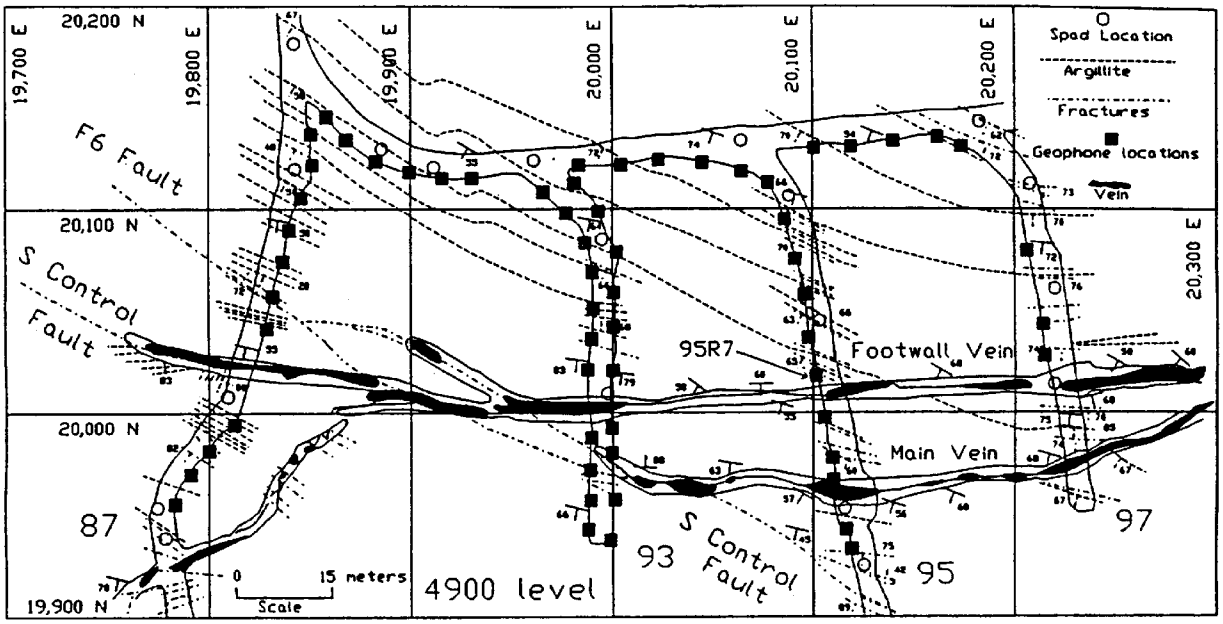
20,200 N
19,700 E
19,800 E
19,900 E
20,000 E
20,100 E
20,200 E
20,300 E
F6 Fault
20,100 N
S Control Fault
95R7
Footwall Vein
20,000 N
Main Vein
87
93
95
97
0 15 meters
Scale
4900 level
19,900 N
S Control Fault
Spad Location
Argillite
Fractures
Geophone locations
Vein

(c)

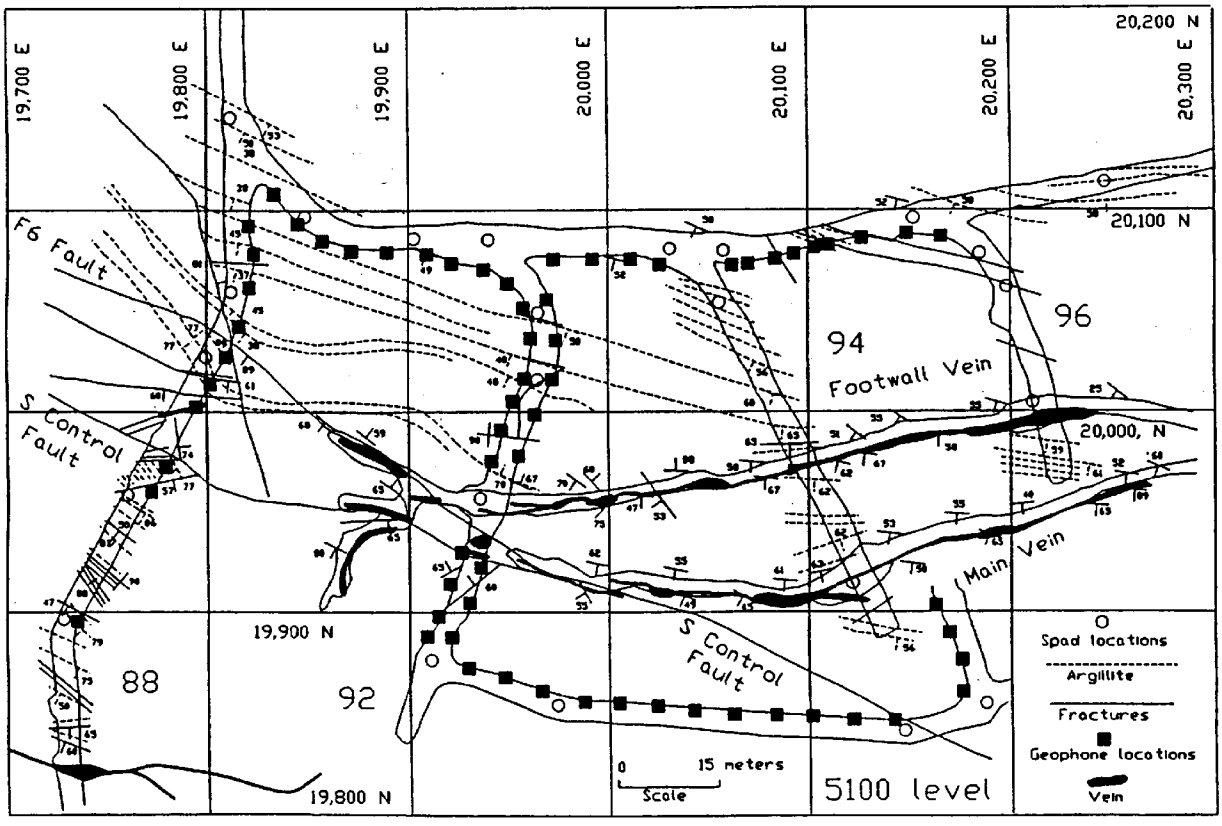
19,700 E
19,800 E
19,900 E
20,000 E
20,100 E
20,200 E
20,300 E
20,200 N
20,100 N
F6 Fault
S Control Fault
94
Footwall Vein
96
20,000, N
Main Vein
19,900 N
88
92
S Control Fault
19,800 N
0 15 meters
Scale
5100 level
Spad locations
Argillite
Fractures
Geophone locations
Vein

(d)

4. Tomographic imaging

4.1. Data acquisition

Seismic energy was introduced by impacting rock bolts along mine drifts using an 8-lb sledge hammer. The first-arriving seismic energy was simultaneously measured at 24 single component 100-Hz geophones. Each geophone was screwed into a rock bolt at locations along the mine drift. Fig. 3(a–d) gives a plan view of geophysical locations at two levels for both mine sites. An instantaneous floating-point seismograph enabled rapid, multichannel, data collection and storage over a 120 dB dynamic range. The signal character was optimized by automatically stacking 20 records (sampled at 0.1-ms intervals), and applying 720 Hz highpass (or lowcut) and 2 kHz anti-aliasing filters. Reciprocity checks were conducted to test the repeatability of timing across and between levels.

4.2. Seismic resolution

The resolution associated with seismic tomography is related to the wavelength of the propagating energy. For transmission tomography, the theoretical resolution is about one wavelength (Williamson, 1991). Knowing the average rock mass velocity (computed from the ensemble of apparent velocities between individual source–reciever pairs), and nominal survey frequency, an estimate of the minimum resolvable limit is determined to be about 7 m. Table 1 gives a summary of the site properties. Thus, if seismic energy is transmitted through high-velocity (high-stress) regions then features larger than this limit should be resolvable. The fact that first-arriving seismic energy preferentially samples high-velocity regions in a heterogeneous domain further enhances our ability to image high-stress regions.

4.3. Grid and initial models

The minimum survey volume was defined as the smallest rectangular parallelepiped enclosing all source and receiver positions, with edges parallel to the mine coordinates. To accommodate the bending of rays outside the minimum survey volume, the computational domain was enlarged by 20%. Calculations for both sites used a uniform grid. A summary of model parameters is presented in Table 2. Note that in both cases the dimensions of individual voxels were comparable to the average wavelength. Also, the number of grid nodes for these surveys is about 2.4–4.4 times greater than the number of travel times resulting in an under-determined system of equations. To reduce the indeterminacy, a global maximum velocity constraint of 6.8 and 6.0 km s^{-1} was imposed during the Homestake and Lucky Friday inversions, respectively. Based on the excellent visual correlation between numerically derived stress and tomographically derived velocity distributions for the first Lucky Friday survey (Friedel et al., 1995b), the remaining three grids were thought to be adequate.

4.4. Inversion

The tomographic reconstructions were obtained by combining iterative adjustment of the alternate starting models, application of global constraints and ray tracing (Jackson and Tweeton, 1996). The

Table 1
Summary of site survey parameters

Date	Survey site	Number of projections, NP	Average velocity (km s^{-1})	Nominal frequency, Hz	Wavelength (m)	Standard error (km s−1)
July 1994	Homestake	1770	5.06	720	7.02	0.120
October 1994	Homestake	2906	5.10	720	7.10	0.090
March 1993	Lucky Friday	2415	3.82	512	7.46	0.078
November 1993	Lucky Friday	4217	4.45	720	6.19	0.068

Table 2
Summary of model parameters

Date	Mine site	Number of nodes, NN	Dimensions[a]	Ratio: NN/NP
July 1994	Homestake	859	9.62 × 8.02 × 3.67	3.87
October 1994	Homestake	6859	9.62 × 8.02 × 3.67	2.36
March 1993	Lucky Friday	10 648	6.40 × 5.20 × 4.30	4.41
November 1993	Lucky Friday	10 648	6.40 × 5.20 × 4.30	2.53

[a]length (m) × width (m) × height (m).

model updates were computed using the simultaneous iterative reconstruction technique, or SIRT (Gilbert, 1972). The velocity distribution resulting from five straight-ray iterations was used as the starting point for the remaining 10 curved-ray iterations. The total number of straight-ray iterations was minimized due to the tendency to diverge from a "best" linear solution (Friedel et al., 1993). Ray tracing was performed by the bending method of Um and Thurber (1987). This approach involves perturbing a trial ray path until the travel time is minimized.

In general, the results reflected a satisfactory global minimum root-mean-square (RMS) travel time residual (about 1.2 and 1.45 ms for the Homestake and Lucky Friday data sets, respectively) and maximum velocity perturbation (RMS difference between starting and updated velocity model) following 15 iterations. RMS residuals were approximately 7.4% (Homestake) and 8.6% (Lucky Friday) of the RMS travel time, and were approximately 30% of those associated with the starting models.

4.5. *Uncertainty*

To evaluate uncertainty associated with the tomographic inversion process, eight different uniform starting velocity models were used to produce a set of reconstructions. These eight reconstructions were viewed as "random" selections from a distribution of possible solutions to the under determined set of equations. In this way, we could use basic probability theory to calculate the likelihood that the true velocity at any node exceeds a threshold value. We selected a value of 6.0 km s^{-1} to represent the critical threshold velocity associated with highly stressed rock. Thus, a node whose average velocity exceeds the threshold value by one or two standard deviations has a probability of 67 or 95% (Abramowitz and Stegun, 1979).

We recognize that the conditions for application of the probability distribution are not rigorously met in this application. Specifically, the eight velocity models on which the statistics are based, although derived from different starting models, are not truly independent estimates of the velocity field, because they are all based on the same travel time measurements. Consequently, the calculated probabilities are overestimated and should not be considered to be quantitative indicators. However, they are useful qualitative guides with respect to the prevailing anomalies.

The degree of uncertainty, for example, associated with the first set of Homestake reconstructions is visually apparent when comparing the 67, 90 and 95% iso-velocity surfaces shown in Fig. 4(a–c). Those velocity anomalies appearing at the 67% iso-velocity periphery are most likely artifacts due to poor raypath coverage and sample density. This assertion is substantiated by the fact that these more uncertain anomalies do not appear in the 90 and 95% iso-velocity figures. The lack of change in velocity structure from 90 to 95% probability implies that either velocity surface may prove sufficient for identifying anomalously high stress regions. Recognizing that a low probability surface incorporates too much tomographic uncertainty, assigning too high a probability value, e.g. 99%, is also unreasonable as there is not enough seismic information available to justify its use. For these reasons, the remaining analyses are based on using 95% iso-velocity surfaces.

4.6. *Stress change due to ground failure*

The computed 3-D iso-velocity surfaces for the Homestake tomographic surveys conducted during

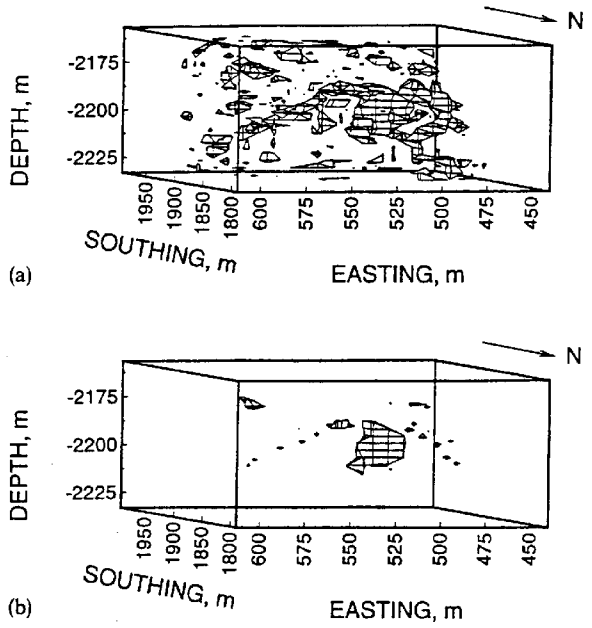

Fig. 4. Iso-velocity surfaces for first tomographic survey at Homestake mine: (a) 67% probability; (b) 90% probability; (c) 95% probability.

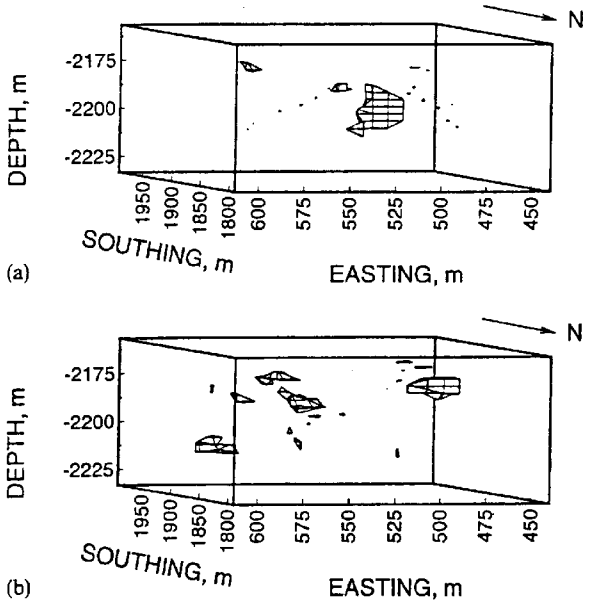

Fig. 5. Three-dimensional iso-velocity surfaces (95% probability) of Homestake mine: (a) tomographic survey 1 (second week July 1993); (b) tomographic survey 2 (third week October 1993).

the second week in July and third week of October are presented in Fig. 5. The variation in spatial high-velocity anomalies (where strain energy is stored) with time is attributed to local changes in the ambient stress field following a 2.2 Richter magnitude seismic event on September 5, 1993. In reviewing the seismic activity (events exceeding 0.5 Richter magnitude) shown in Fig. 6, the first survey was conducted during a period of low but constant rate of seismicity (four events per month). Following another 2-month period, the seismicity increased with continued stope mining to 11 events per month when a 2.2 Richter magnitude seismic event occurred. Between the time of this event and second survey, the seismicity increased from three to 19 events per month. This increased rate of seismicity is attributed to a redistribution in the stress field further supporting the tomographic interpretation.

4.7. Stress change due to stope advancement

Velocity histograms for the two Lucky Friday mine surveys conducted in the first week of March

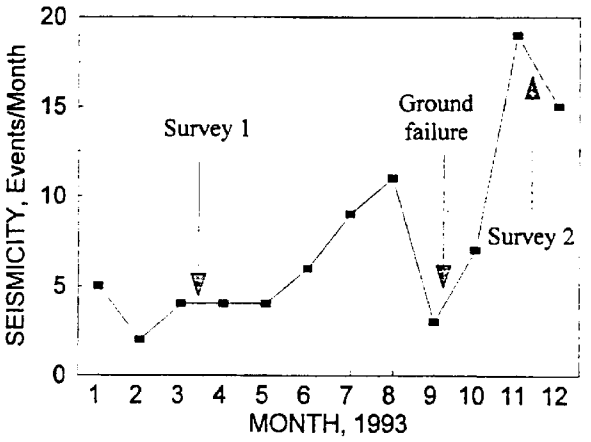

Fig. 6. Seismic activity (Richter magnitude exceeding 0.5) at Homestake mine.

and second week of November 1993 are shown in Fig. 7. In contrast to the Homestake mine, there is a statistically significant increase in average site velocity (from 3.82 to 4.45 km s^{-1}). The increase in apparent velocity is consistent with a model of stress transfer from the lower mined-out portions of veins to the upper intact remnant ore structure.

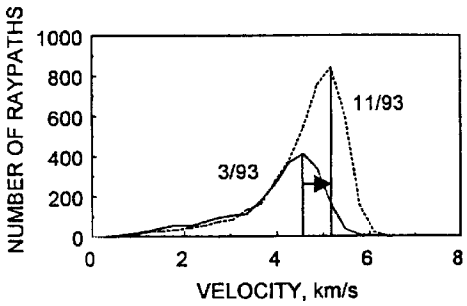

Fig. 7. Velocity histograms for Lucky Friday mine during first week March and second week November, 1993.

This is particularly true in view of the abnormally high horizontal to vertical stress ratio of 2. While comparison of these average velocity values provides some qualitative information regarding increasing stress in the survey region, it cannot differentiate its spatial location.

To identify and monitor changing stress conditions in the remnant ore pillar, seismic data from the tomographic surveys were used to produce the high (opaque) and low (translucent) iso-velocity surfaces shown in Fig. 8(a,b). In addition to the velocity surfaces, Fig. 8 also provides a 3-D rendering of the silver vein and corresponding mine drifts. Like the Homestake mine, the Lucky Friday mine also experienced a catastrophic release of strain energy. This 3.5 Richter magnitude event occurred 1 month prior to the first survey and damaged select regions on both the 4900 and 5100 levels. The damaged regions are outlined in the figure and appear as translucent, low velocity (low stress), anomalies surrounding the drift.

It is interesting to note the disappearance of the low-velocity anomaly in the region of ground failure on the lower 5100 level. This apparent increase in velocity further indicates an apparent transfer of stress from below to the remnant structure during stope advancement. The long low velocity anomaly, parallel to the crosscut drifts on the lower level, is actually a drift that sustained severe damage during the release of stored strain energy. The ability to image this drift during the second survey is due to increased tomographic coverage. While the other drifts remain open, this "ghost" drift was backfilled in an attempt to mitigate future stability problems.

Another indication of apparent stress transfer due to mining activity is the increase in the volume of high velocity. For example, as mining progressed downward (from March to November), the volume of critically stressed rock appears to have expanded by more than a factor of 2. The concentration of stress along the hanging wall side of the veins suggests that it may be exerting some degree of structural control.

5. Discussion and conclusions

The velocity structure we have imaged can be interpreted qualitatively in terms of stress anomalies, in a way that is broadly consistent with measured in situ stresses. Reconstructed regions of low velocity correlate with locations of stress-relieved zones surrounding drifts and sites that experienced catastrophic ground failure. Iso-probability maps show robust high-velocity anomalies and provide the best estimate of the locations of anomalously high-stress regions.

Various factors should be borne in mind when interpreting the relationships between p-wave velocity, stress, and in attempts to evaluate ground stability hazards using such observations. First, we have used the term "stress" quite generally, without distinguishing between hydrostatic and differential stresses or their orientations. A related limitation lies in our treatment of velocity as isotropic, which may produce artifacts in the reconstructions if anisotropy is significant.

Despite these limitations, the final velocity reconstructions are consistent with all available "ground truth" information; even difficult-to-image low-velocity features such as regions that experienced ground failure are accurately represented. We therefore consider the final model as a limited but nevertheless essential tool for ground stability hazard evaluation. In particular, large releases of strain energy affect rock volumes with dimensions many times larger than the 7-m dominant wavelength of this study, and anomalous stress variations on such a scale are more amenable to accurate tomographic reconstruction.

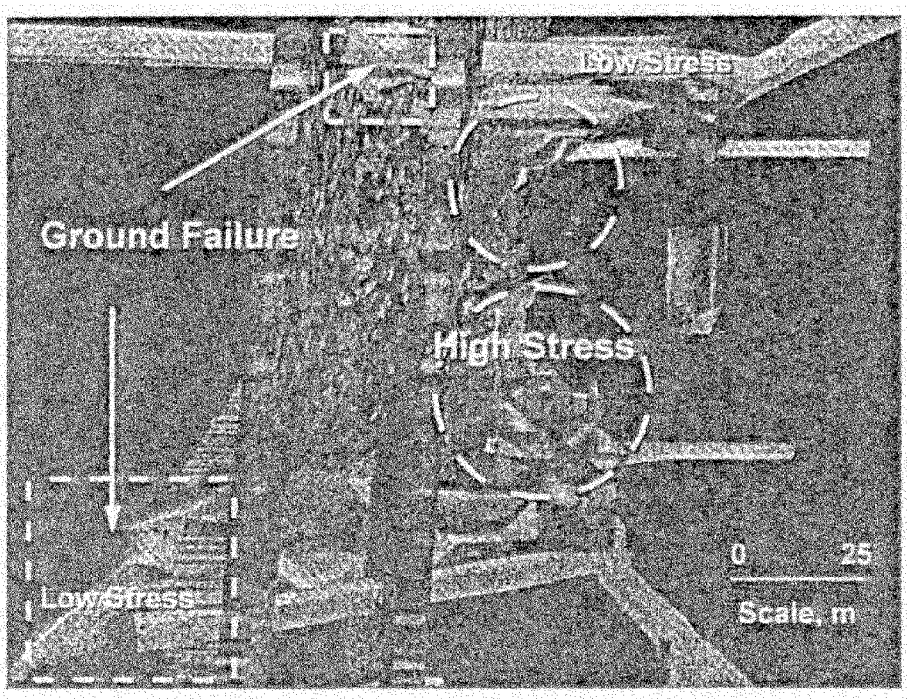

(a)

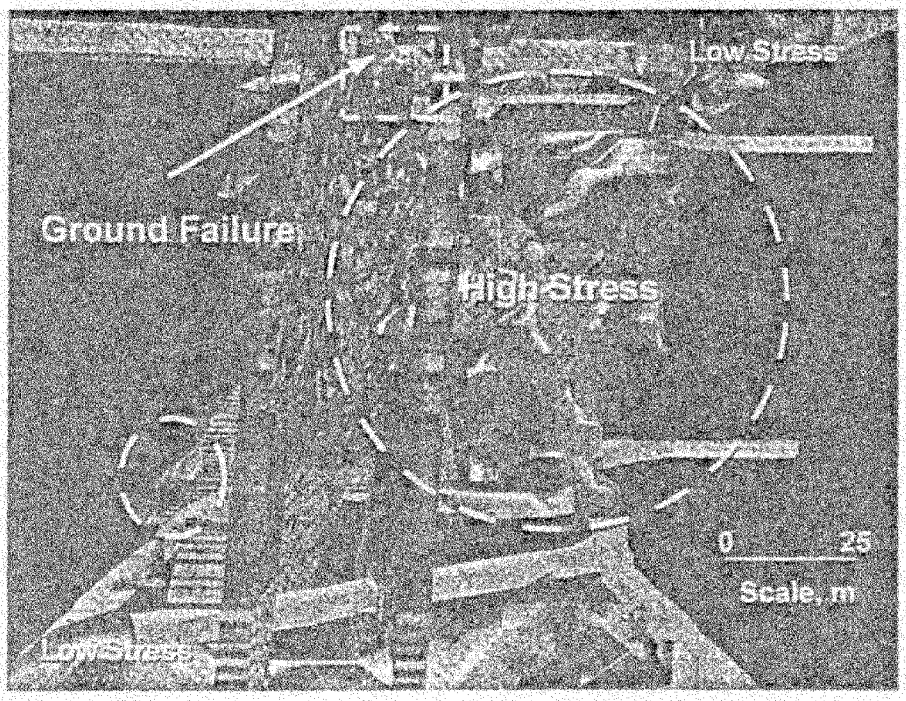

(b)

Fig. 8. Three-dimensional iso-velocity surfaces (95% probability) of Lucky Friday mine: (a) tomographic survey 1 (first week March 1993); (b) tomographic survey 2 (second week November 1993).

Acknowledgment

The authors thank the management of Homestake and Hecla mining companies for providing underground access and information related to ground failure and seismic activity.

References

Abramowitz, M. and Stegun, I.A., 1979. Handbook of Mathematical Functions. Dover, New York.

Blake, W. and Cuvelier, D., 1990. Developing reinforcement requirements for rock burst conditions at Hecla's Lucky Friday mine. Proc. 2nd Int. Symp. Rock Bursts and Seismicity in Mines '88, Balkema, Rotterdam, pp. 407–409.

Friedel, M.J., Tweeton, D.R., Jackson, M.J., Jessop, J.A. and Billington, S., 1992. Mining applications of seismic tomography. Expanded Abstracts, Ann. Int. Mtg, Soc. Expl. Geophys., New Orleans, LA, October 25–28, pp. 58–62.

Friedel, M.J., Jackson, M.J., Tweeton, D.R. and Olson, M.S., 1993. Application of seismic tomography for assessing yield pillar stress conditions. Proc. Twelfth Int. Conf. Ground Control Min., Morgantown, WV, August, pp. 292–300.

Friedel, M.J., Jackson, M.J. and Williams, E.M., 1995a. Tomographic imaging of coal pillar behavior: observations and implications. Int. J. Rock Mech. Min. Sci., 33(1), 1995.

Friedel, M.J., Jackson, M.J., Scott, D.F., Williams, T.J. and Olson, M.S., 1995b. 3D tomographic imaging of anomalous conditions in a deep silver mine. J. Appl. Geophys., 34(1), 1–21.

Friedel, M.J., Scott, D.F., Jackson, M.J., Williams, T.J. and Killen, S.M. 1996. 3D tomographic imaging of anomalous stress conditions in a gold mine. J. Appl. Geophys., (in press).

Gibowicz, S.J. and Kijko, A., 1994. An Introduction to Mining Seismology. Academic Press, San Diego, 399 pp.

Gilbert, P., 1972. Iterative methods for the three-dimensional reconstruction of an object from projections. J. Theoret. Biol., 36, 105–117.

Jackson, M.J. and Tweeton, D.R., 1996. 3DTOM — Three Dimensional Geophysical Tomography, BuMines RI 9617, 84 pp.

Johnson, J.C., Pariseau, W.G., Scott, D.F. and Jenkins, F.M., 1993. In situ stress measurements near the Ross shaft pillar. BuMines RI 9446, 17 pp.

Maxwell, S.C. and Young, R.P., 1992. 3D seismic velocity imaging using microseismic monitoring systems at Strathcona mine and mines gaspe, Proc. 94th AGM, Canadian Institute of Mining.

McCreary, R., McGaughey, J., Potvin, Y., Ecobichon, D., Hudyma, M., Kanduth, H. and Coulombe, A., 1992. Results from microseismic monitoring, conventional instrumentation, and tomography surveys in the creation and thinning of a burst-prone still pillar. PAGEOPH, 139, 349–373.

Radcliffe, K.S., Thill, R.E. and Jessop, J.A., 1986. Use of acoustic velocity for predicting stress under uniaxial compression. 115th Ann. AIME Mtg. Reprint 86–147, 11 pp.

Scott, D.F., 1993. Geologic investigation near an underhand cut-and-fill stope, Lucky Friday mine, Mullan, ID, BuMines RI, 9470, 25 pp.

Thill, R.E., 1982. Coal and rock properties for premine planning and mine design. BuMines IC 8973, pp. 15–35.

Um, J. and Thurber, C., 1987. A fast algorithm for two-point seismic ray tracing. Bull. Seismol. Soc. Am., 77, 972–986.

Westmann, E.C., Foss, M.M. and Williams, E.M., 1994. Comparison of stress distribution images generated with P, Sh and SV velocity tomograms. Expanded Abstracts, Ann. Int. Mtg. Soc. Expl. Geophys., Los Angeles, CA, October 23–28.

Williamson, P.R., 1991. A guide to the limits of resolution imposed by scattering in ray tomography. Geophys., 56(2), 202–207.

Young, R.P., (Editor), 1993. Rock Bursts and Seismicity in Mines '93, A.A. Balkema, Rotterdam.

Young, R.P. and Hill, J.J., 1985. Seismic characterization of rock masses before and after mine blasting. Proc. 26th US Symp. Rock Mech., Rapid City (SD), pp. 1151–1158.

Young, R.P. and Maxwell, S.C., 1992. Seismic characterization of a highly stressed rock mass using tomographic imaging and induced seismicity. J. Geophys. Res., 97, 12361–12373.